

## Supplementary Material for

# Copper(II) binding to PBT2 differs from that of other 8-hydroxyquinoline chelators: Implications for the treatment of neurodegenerative protein misfolding diseases

*Kelly L. Summers,\* Graham Roseman, George Sopasis, Glenn L. Millhauser, Hugh H. Harris,*

*Ingrid J. Pickering,\* Graham N. George*

\*Co-corresponding authors: K. L. Summers, [kelly.summers@usask.ca](mailto:kelly.summers@usask.ca); I. J. Pickering, [ingrid.pickering@usask.ca](mailto:ingrid.pickering@usask.ca); G. N. George, [g.george@usask.ca](mailto:g.george@usask.ca)

## Contents

Hydrophobicity of PBT2 and its Cu(II) Complex .....	S3
UV–Visible Absorption Spectroscopy Methods .....	S3
UV-Visible Absorption Spectroscopy .....	S4
Density Functional Theory Calculations .....	S5
References .....	S14

## Figures

Figure S1. UV-visible absorption spectra of PBT2 titration with Cu(II) .....	S4
Figure S2. DFT geometry optimized structures of Cu(II) complexes of 5,7-dichloro-8-hydroxyquinoline and its derivatives.....	S7
Figure S3. Comparison of conventional XAS (dashed line) and HERFD-XAS (solid line) near-edge spectra of excess PBT2: Cu .....	S8
Figure S4. Conventional XAS spectra of a Cu(II) titration with PBT2.....	S8
Figure S5. Diagram of angles for Cu(II) 8HQ complexes listed in Table S.2.....	S9
Figure S6. Examples of alternative fits for EXAFS spectra and Fourier transforms of the Cu(II) complex with PBT2.....	S11

## Tables

Table S1. UV-visible absorption data for 8-hydroxyquinoline and its derivatives, CQ and PBT2, and their complexes with Cu(II) in surfactant solution.....	S5
Table S2. Calculated angles from geometry optimized Cu(II) 8HQ complexes .....	S10
Table S3. Alternative Cu K-edge EXAFS curve fitting results for the Cu(II) solution with excess PBT2 .....	S12
Table S4. Best fit Cu K-edge EXAFS curve fitting results for the Cu(II) solution with excess PBT2 and the solution with 1 PBT2: 1 Cu(II) .....	S13

## Hydrophobicity of PBT2 and its Cu(II) Complex

The hydrophobicity of 8HQ, and its derivatives and their complexes with Cu(II), has been shown to correlate with cytotoxicity in cancer cell lines,<sup>1</sup> and the hydrophobicity of some 8HQ complexes with divalent metals has been linked with their ionophoric action.<sup>2</sup> However, the hydrophobicity of these complexes have also made the study of these complexes difficult without the use of organic solvents, and even using solvents, precipitation of these complexes is frequently reported.<sup>1, 3-9</sup> We have calculated the partition coefficient,  $\log P$ , as a measure of hydrophobicity of PBT2 and its complexes with Cu(II).  $\log P$  is often used to estimate the hydrophobicity of candidate drug compounds and predict the behavior of these compounds in the body since hydrophobicity can be a major determining factor for absorption, distribution, membrane penetration, metabolism and excretion. Generally, the ideal  $\log P$  of a compound intended for oral administration is thought to be 5, according to Lipinski's Rule of Five.<sup>10</sup> The  $\log P$  value of PBT2 was found to be 3.23, and the  $\log P$  of the Cu(II)-*bis*-PBT2 complex was 6.15, which is in line with 5,7-dichlorinated-8-hydroxyquinolines investigated previously,<sup>11</sup> and which could suggest that the Cu(II)-*bis*-PBT2 complex is more biologically active than PBT2 alone.

## UV-Visible Absorption Spectroscopy Methods

UV-visible absorption spectra were collected using a Varian Cary 50 and Cary WinUV Scan software. A stock solution of 1 mM CuCl<sub>2</sub> was prepared in diH<sub>2</sub>O. An aqueous 1 mM stock solution of PBT2 was prepared in 400 mM DTAB and 100 mM MOPS at pH 7.5 and diluted to 250  $\mu$ M in diH<sub>2</sub>O. CuCl<sub>2</sub> was added to final concentrations of 50, 125, and 250  $\mu$ M for spectra of the 1:5, 1:2, and 1:1 Cu(II)/PBT2 solutions, respectively. Data was collected from 800–200 nm on 1 mL samples in 1 cm quartz cuvettes. Spectra were baseline corrected using 100 mM DTAB in 25 mM MOPS at pH 7.

## UV-Visible Absorption Spectroscopy

The UV-visible absorption spectra of the Cu(II) PBT2 complex has been published previously and used to suggest that PBT2 binds Cu(II) in a 1:1 ratio.<sup>4, 12</sup> In this study, Cu(II) was titrated into an aqueous solution of PBT2 and UV-visible absorption spectra were collected (Figure S.1; Table S.1). The resulting spectra appear somewhat similar to those previously published for PBT2<sup>3, 4</sup> and similar ligands.<sup>12, 13</sup> Differences might be attributed to differences in solution composition since these complexes have been shown previously to be sensitive to solution conditions, particularly solvent polarity.<sup>14, 15</sup> UV-visible absorption spectra also look similar to spectra published previously for other Cu(II)-*bis*-8HQ complexes in aqueous solution,<sup>11</sup> with the exception that the shorter wavelength transition typically has a shoulder, which is lacking in most PBT2 complex spectra (Figure S.1).

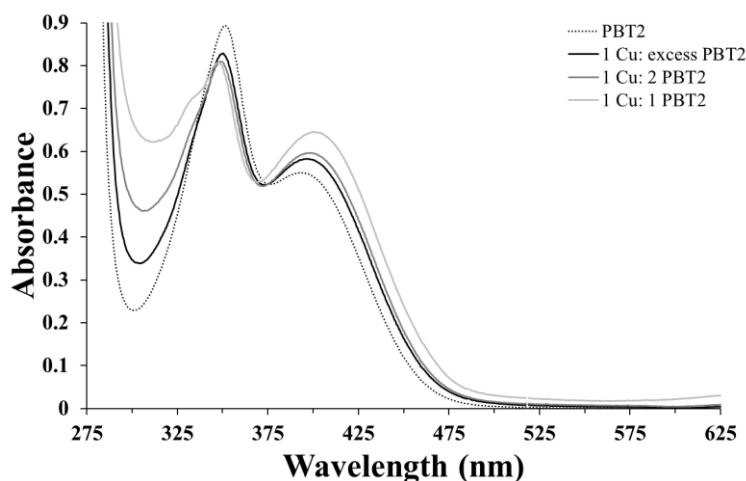


**Figure S1. UV-visible absorption spectra of PBT2 titration with Cu(II).**

**Table S1. UV-visible absorption data for 8-hydroxyquioline and its derivatives, CQ and PBT2, and their complexes with Cu(II) in surfactant solution.**

Compound	Free Ligand		Complexed with Cu(II)*			
	$\lambda_{\max}$ (nm)	$\epsilon$ ( $M^{-1} \text{ cm}^{-1}$ )	$\lambda_{\max < 370 \text{ nm}}$	$\epsilon$ ( $M^{-1} \text{ cm}^{-1}$ )	$\lambda_{\max > 370 \text{ nm}}$	$\epsilon$ ( $M^{-1} \text{ cm}^{-1}$ )
CQ <sup>a</sup>	345	1179	<b>349</b>	1555	411	493
Cl2Q <sup>a</sup>	344	2181	<b>345</b>	2081	401	1649
MC2Q <sup>a</sup>	324	950	<b>330</b>	953	399	252
5 PBT2: 1 Cu	352	3571	<b>353</b>	3243*	403	2293*
2 PBT2: 1 Cu			<b>350</b>	3229*	400	2382*
1 PBT2: 1 Cu			<b>347</b>	3223*	388	2446*

bold values = true  $\lambda_{\max}$ ; <sup>a</sup> values from Summers *et al.*<sup>11</sup> in the same buffered surfactant solutions;  
\* calculated based on the concentration of PBT2 which was kept constant during the titration

## Density Functional Theory Calculations

In Cu(II) complexes of previously studied 8HQs, the electron density of the HOMO was found to be concentrated on the ligand atoms, particularly the phenolic oxygens and the ligand  $\pi$  system with some minor contribution from the Cu  $3d_{yz}$  orbitals. Conversely, the LUMO had larger contributions from the Cu  $3d_{x^2-y^2}$  orbitals, as well as contributions from the nitrogen and oxygen ligands. The HOMO to LUMO transition was therefore proposed to be from a predominantly ligand-based orbital to an orbital with significant contributions from Cu  $3d$  orbitals.<sup>11</sup> Substitution of 2-CHO in the 2-position of 5,7-dichloro-8HQ resulted in some of the electron density of the HOMO being pushed onto the 2-position O of 2-CHO, but overall the HOMO to LUMO transition was not significantly altered in AC2Q.<sup>11</sup> In the 2 N 2 O distorted 4-coordinate Cu(II)-*bis*-PBT2 complex described above, the HOMO was similarly concentrated on the ligand atoms, particularly the phenolic oxygens and the ligand  $\pi$  system again with some minor contribution from the Cu  $3d_{yz}$  orbitals; however, more significant contributions from the 2-position tertiary amine are noted in this complex compared with the 2-CHO substitution in AC2Q (Figure S.2). The LUMO also

similarly had larger contributions from the Cu  $3d_{x^2-y^2}$  orbitals and from the phenolate oxygen and pyridine nitrogen ligands. The HOMO to LUMO transition is also proposed to be from a largely ligand-based orbital to an orbital with significant Cu  $3d$  contributions. For the 3 N 1 O highly distorted Cu(II)-*bis*-PBT2 complex, the HOMO and LUMO are accompanied by orbitals with similar isosurfaces that are close in energy, but localized on the other heterocycle. There are also greater contributions from the coordinating tertiary amine to the HOMO compared with the non-coordinating tertiary amine ([Figure S.2](#)). The LUMO appears to have greater contributions from the ligand  $\pi$  system, compared with other 2 N 2 O structures ([Figure S.2](#)). Taken together, these findings suggest that the electronic distribution is considerably altered in the 3 N 1 O coordination environment in Cu(II)-*bis*-PBT2.

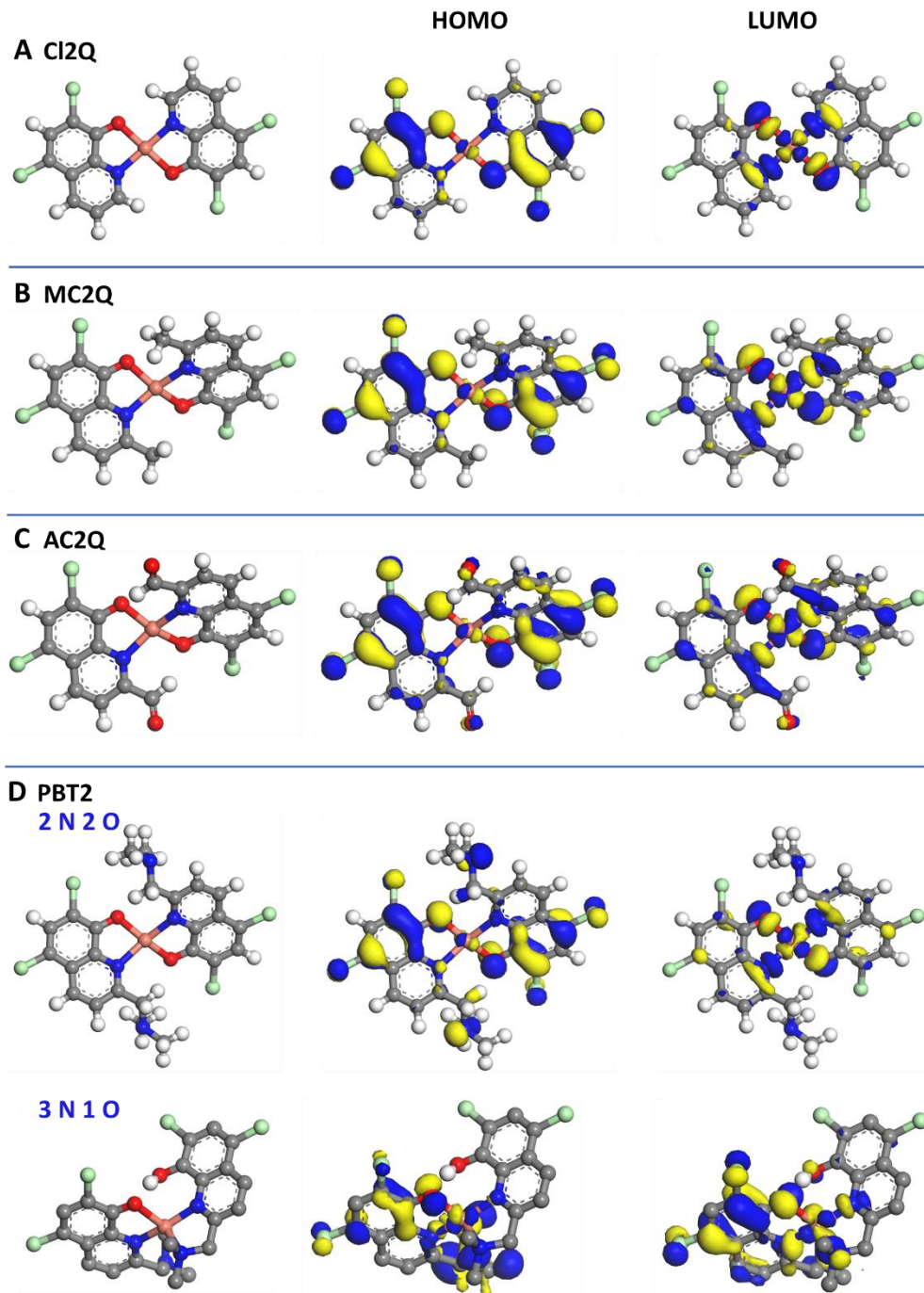


**Figure S2. DFT geometry optimized structures of Cu(II) complexes of 5,7-dichloro-8-hydroxyquinoline and its derivatives.** Isosurface plots of the HOMO and LUMO are shown in blue and yellow. A conventional color scheme was chosen for each element, such that hydrogen is white, carbon is grey, nitrogen is blue, oxygen is red, copper is shown in pink, and chlorine is shown in green. For the *cis* 3 N 1 O Cu(II) coordination complex with PBT2, the hydrogens were included in the calculations, but are omitted from the figure for clarity (with the exception of the proton on the 8-position oxygen). There is another set of near-degenerate orbitals with electron density on the other heterocycle of the 3 N 1 O PBT2 complex (not shown).

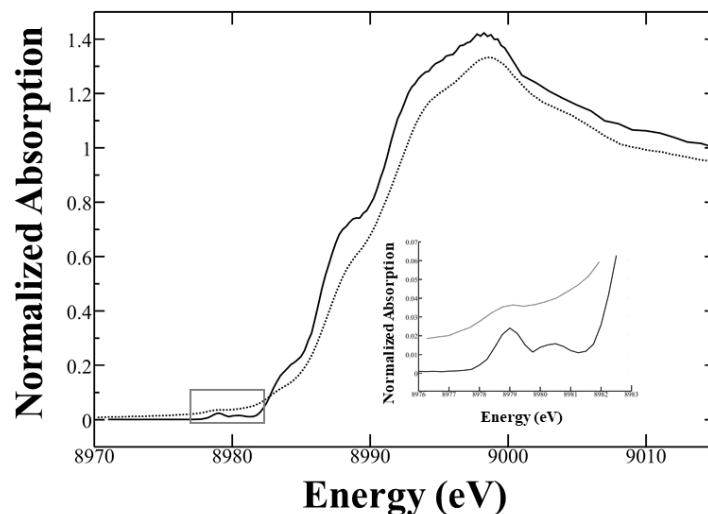


**Figure S3. Comparison of conventional XAS (dashed line) and HERFD-XAS (solid line) near-edge spectra of excess PBT2: Cu.** Inset shows the  $1s \rightarrow 3d$  region highlighted by the box. For Cu(II) complexes the  $1s \rightarrow 3d$  is typically a single peak centered at approximately 8979.0 eV; however, the HERFD-XAS spectrum shows a second peak at ~8980.4 eV.

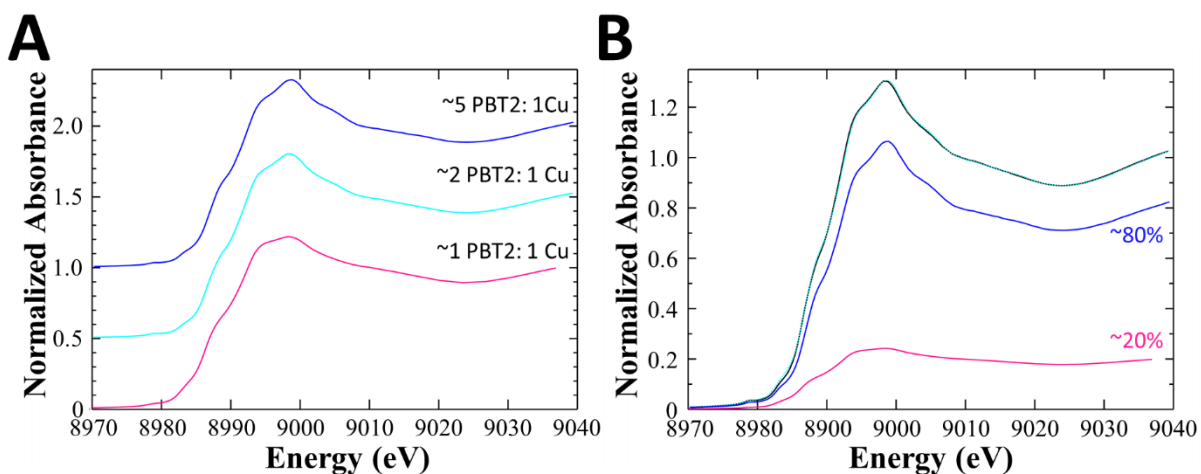


**Figure S4. Conventional XAS spectra of a Cu(II) titration with PBT2.** (A) Near-edge spectra of 5 PBT2: Cu(II) (dark blue), 2 PBT2: 1 Cu(II) (light blue), and 1 PBT2: 1 Cu (pink). Spectra are offset by 0.5 vertically. (B) Near-edge fit of the 2 PBT2: 1 Cu spectrum (dashed line) with 80% of the excess PBT2: Cu(II) spectrum and 20% of the 1 PBT2: 1 Cu(II) spectrum.

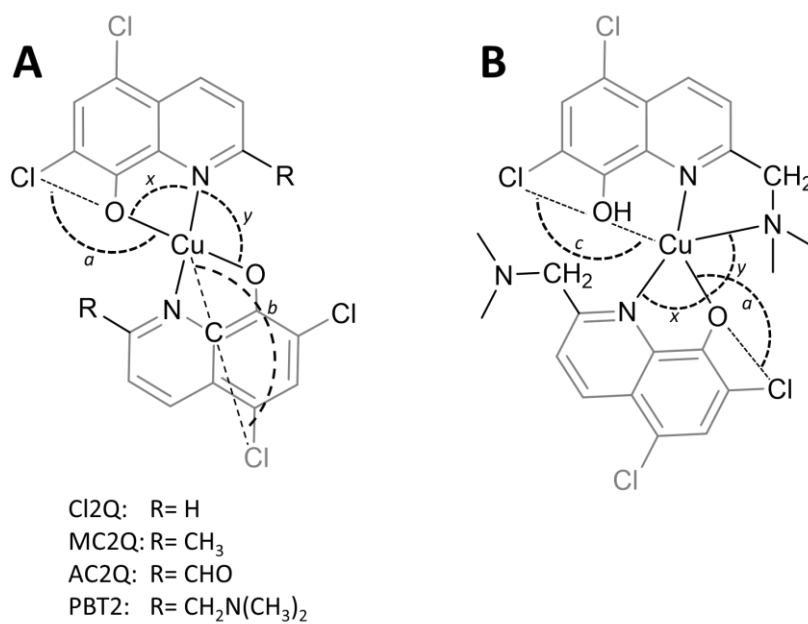


**Figure S5. Diagram of angles for Cu(II) 8HQ complexes listed in Table S.2.** (A) Schematic of typical 4-coordinate *trans* Cu(II)-*bis*-8HQ complexes. (B) Schematic of the 3 N 1 O Cu(II)-*bis*-PBT2 complex.

**Table S2. Calculated angles from geometry optimized Cu(II) 8HQ complexes.<sup>a</sup>**

Cu(II)-bis-8HQ	O–Cu–O Angle <sup>b</sup>	N–Cu–N Angle	O–Cu–N Angle <sup>c</sup>	O–Cu–N' Angle <sup>d</sup>	Cu–O···Cl Angle <sup>e</sup>	Cu–O···Cl' Angle <sup>f</sup>	Cu···C···Cl Angle <sup>g</sup>	Cu···C···Cl' Angle <sup>h</sup>	$\tau^4$	$\tau^{4'}$	2-Subst.
Cl2Q <sup>j</sup>	180.00	180.00	84.13	95.87	174.36		176.92		0.00	0.00	-H
MC2Q <sup>j</sup>	150.34	156.53	83.94	102.09	175.99		175.10		0.38	0.36	-CH <sub>3</sub>
AC2Q <sup>j</sup>	148.70	153.81	83.44	103.68	175.99		174.96		0.41	0.39	-CHO
PBT2											
2 N 2 O	150.45	154.98	83.55	102.87	176.45		174.69		0.39	0.37	-CH <sub>2</sub> N(CH <sub>3</sub> ) <sub>2</sub>
3 N 1 O	64.19	158.82	82.13 <sup>k</sup>	104.06 <sup>k</sup>	174.10	166.75	175.76	169.88	0.97	0.68	-CH <sub>2</sub> N(CH <sub>3</sub> ) <sub>2</sub>

<sup>a</sup> all angles in degrees; <sup>b</sup> O–Cu···O angle in 3 N 1 O PBT2; <sup>c</sup> depicted angle *x* in Figure S.4; <sup>d</sup> depicted angle *y* in Figure S.4; <sup>e</sup> depicted angle *a* in Figure S.4; <sup>f</sup> depicted angle *c* in Figure S.4 B; <sup>g</sup> angle *b* in Figure S.4 A; <sup>h</sup> of the 2N-donating PBT2 ligand; <sup>j</sup> from Summers *et al.*<sup>11</sup>; <sup>k</sup> only formed with one PBT2 chelate (see Figure S.4 B).  $\tau^4$  and  $\tau^{4'}$  parameters calculated as [described by Yang \*et al.\*<sup>16</sup>](#) and [Okuniewski \*et al.\*<sup>17</sup>](#) respectively.

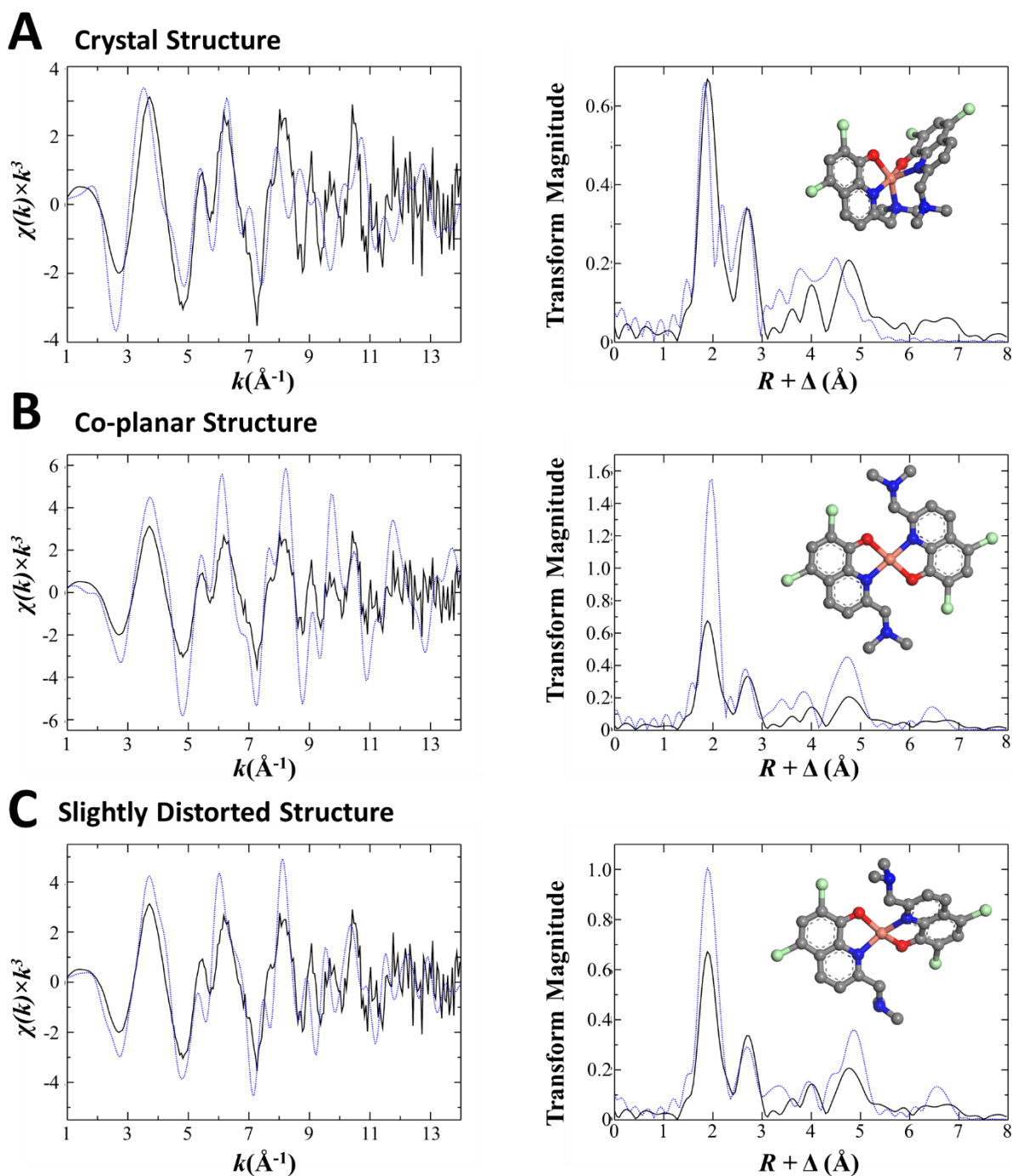


**Figure S6. Examples of alternative fits for EXAFS spectra and Fourier transforms of the Cu(II) complex with PBT2.** Inset shows the geometry optimized structure used to generate the multiple scattering paths for the fit. Hydrogens are omitted for clarity. Fitting parameters are listed in Table S.3.

**Table S3. Alternative Cu K-edge EXAFS curve fitting results for the Cu(II) solution with excess PBT2.<sup>a</sup>**

<b>Cu(II)-bis-PBT2 Crystal Structure</b>					
<b>Path</b>	<b><i>N</i></b>	<b><i>R</i></b>	<b><math>\sigma^2</math></b>	<b><math>\Delta E_0</math></b>	<b><i>F</i></b>
Cu–O	1	1.909	0.0028	-1.2(4)	0.8233
Cu–N	1	1.914	0.0031		
Cu–O	1	2.052	0.0029		
Cu–N	1	2.113	0.0033		
Cu–N <sub>amino</sub>	1	2.229	0.0034		
Cu···N <sub>amino</sub>	1	3.800	0.0034		
<i>73 unlisted multiple scattering paths</i>					
Cu···Cl	1	4.833	0.0048		
Cu···Cl···O	2	4.849	0.0048		
Cu···O···Cl···O	1	4.864	0.0049		
Cu···Cl	1	5.081	0.0048		
Cu···Cl···O	2	5.086	0.0048		
Cu···O···Cl···O	1	5.093	0.0048		
<b>Co-planar Cu(II)-bis-PBT2 Structure</b>					
<b>Path</b>	<b><i>N</i></b>	<b><i>R</i></b>	<b><math>\sigma^2</math></b>	<b><math>\Delta E_0</math></b>	<b><i>F</i></b>
Cu–O	2	1.964(4)	0.0028	-3.0(7)	1.2092
Cu–N	2	2.018	0.0032		
Cu···N <sub>amino</sub>	2	4.710	0.0035		
<i>44 unlisted multiple scattering paths</i>					
Cu···Cl	2	4.925	0.0048		
Cu···Cl···O	4	4.926	0.0048		
Cu···O···Cl···O	2	4.926	0.0048		
Cu···Cl	2	6.664	0.0047		
Cu···C···Cl	4	6.664	0.0047		
<b>Distorted Cu(II)-bis-PBT2 Structure</b>					
<b>Path</b>	<b><i>N</i></b>	<b><i>R</i></b>	<b><math>\sigma^2</math></b>	<b><math>\Delta E_0</math></b>	<b><i>F</i></b>
Cu–O	2	1.909(5)	0.0028	-2.8(7)	0.8293
Cu–N	2	2.048(6)	0.0033		
Cu···N <sub>amino</sub>	2	4.753	0.0035		
<i>39 unlisted multiple scattering paths</i>					
Cu···Cl	2	5.012	0.0048		
Cu···Cl···O	4	5.014	0.0048		
Cu···O···Cl···O	2	5.015	0.0048		
Cu···Cl	2	6.721	0.0040		
Cu···C···Cl	4	6.771	0.0040		

<sup>a</sup> Corresponding plots are shown in Figure S.5. Possible fitting parameters included the distance between absorbing atom (i.e. Cu) and the backscattering atom (*R*) and the energy offset to the threshold energy ( $\Delta E_0$ ). The values in parentheses are the estimated standard deviations (e.s.d.) obtained from the diagonal elements of the covariance matrix for *R*,  $\sigma^2$ , and  $\Delta E_0$ . Estimated e.s.d.

values correspond to the error on the last digit. Coordination numbers  $N$  and mean square deviations in  $R$  (Debye-Waller factor;  $\sigma^2$ ) were held fixed in the refinements. Values without e.s.d., apart from  $N$  values, were either held fixed or were refined as a set of parameters linked by constant proportion to those of the Cu-O/ $N$  paths and the e.s.d. will correspond to that of Cu-O/ $N$ . The  $F$  value is a goodness of fit value calculated as described in the methods.

**Table S4. Best fit Cu K-edge EXAFS curve fitting results for the Cu(II) solution with excess PBT2 and the solution with 1 PBT2: 1 Cu(II).<sup>a</sup>**

<b>Best Fit Excess PBT2: Cu(II)</b>						
<b>Path</b>	<b><math>N</math></b>	<b><math>R</math></b>	<b><math>\sigma^2</math></b>	<b><math>\Delta E_0</math></b>	<b><math>F</math></b>	<b><math>F'</math></b>
Cu–O	2	1.909(4)	0.0054(3)	-3.1(5)	0.5073	0.2230
Cu–N	2	2.082	0.0058			
Cu···N <sub>amino</sub>	2	4.715	0.0077			
<i>63 unlisted multiple scattering paths</i>						
Cu···Cl	2	4.952	0.0075			
Cu···Cl···O	4	4.953	0.0075			
Cu···O···Cl···O	2	4.954	0.0075			
Cu···Cl	2	6.493	0.0056			
Cu···C···Cl	4	6.943	0.0056			
<b>Best Fit 1 PBT2: 1 Cu(II)</b>						
Cu–O	1	1.902(4)	0.0040(2)	-6.1(8)	0.4059	0.1948
Cu–N	1	2.046	0.0044			
Cu–N <sub>amino</sub>	1	2.190	0.0048			
Cu–Cl	1	2.225	0.0023			
<i>54 unlisted multiple scattering paths</i>						
Cu···Cl	1	5.058	0.0069			
Cu···Cl···O	2	5.064	0.0070			
Cu···O···Cl···O	1	5.070	0.0070			
Cu···Cl	1	6.574	0.0021			
Cu···C···Cl	2	6.874	0.0021			

<sup>a</sup> Corresponding best fit plots are shown in Figure 7. Fitting parameters included the following: distance between absorbing atom (i.e. Cu) and the backscattering atom ( $R$ ), mean square deviation in  $R$  (Debye-Waller factor;  $\sigma^2$ ), and the energy offset to the threshold energy ( $\Delta E_0$ ). The values in parentheses are the estimated standard deviations (e.s.d.) obtained from the diagonal elements of the covariance matrix for  $R$ ,  $\sigma^2$ , and  $\Delta E_0$ . Estimated e.s.d. values correspond to the error on the last digit. Coordination numbers  $N$  were held fixed in the refinements. Values without e.s.d., apart from  $N$  values, were refined as a set of parameters linked by constant proportion to those of the Cu–O/ $N$  paths and the e.s.d. will correspond to that of Cu–O/ $N$ . The  $F$  and  $F'$  values are goodness of fit values calculated as described in the methods.

## References

1. Tardito, S., Barilli, A., Bassanetti, I., Tegoni, M., Bussolati, O., Franchi-Gazzola, R., Mucchino, C., and Marchio, L. (2012) Copper-dependent cytotoxicity of 8-hydroxyquinoline derivatives correlates with their hydrophobicity and does not require caspase activation, *J. Med. Chem.* *55*, 10448-10459.
2. Tjälve, H., and Ståhl, K. (1984) Effect of 5-chloro-7-iodo-8-hydroxyquinoline (Clioquinol) on the uptake and distribution of nickel, zinc and mercury in mice, *Acta Pharmacol. Toxicol. (Copenh.)* *55*, 65-72.
3. Sgarlata, C., Arena, G., Bonomo, R. P., Giuffrida, A., and Tabbi, G. (2018) Simple and mixed complexes of copper(II) with 8-hydroxyquinoline derivatives and amino acids: Characterization in solution and potential biological implications, *J. Inorg. Biochem.* *180*, 89-100.
4. Nguyen, M., Vendier, L., Stigliani, J.-L., Meunier, B., and Robert, A. (2017) Structures of the copper and zinc complexes of PBT2, a chelating agent evaluated as potential drug for neurodegenerative diseases, *Eur. J. Inorg. Chem.*, 600-608.
5. Albert, A., Gibson, M. I., and Rubbo, S. D. (1953) The influence of chemical constitution on anti-bacterial activity. Part VI: The bactericidal action of 8-hydroxyquinoline (oxine), *Br. J. Exp. Pathol.* *34*, 119-130.
6. Hollingshead, R. G. W. (1954) *Oxine*, Vol. I, Butterworths Scientific Publications, London.
7. Budimir, A., Humbert, N., Elhabiri, M., Osinska, I., Biruš, M., and Albrecht-Gary, A.-M. (2011) Hydroxyquinoline based binders: Promising ligands for chemotherapy, *J. Inorg. Biochem.* *105*, 490-496.
8. Welcher, F. J. (1947) Quinoline and quinoline derivatives, In *Organic Analytical Reagents*, p 49, D. Van Nostrand Company, Inc.
9. Phillips, J. P. (1956) The reactions of 8-quinolinol, *Chem. Rev.* *56*, 271-297.
10. Lipinski, C. A., Lombardo, F., Dominy, B. W., and Feeney, P. J. (2001) Experimental and computational approaches to estimate solubility and permeability in drug discovery and development settings, *Adv. Drug Del. Rev.* *46*, 3-26.
11. Summers, K. L., Pushie, M. J., Sopasis, G. J., James, A. K., Dolgova, N. V., Kroll, T., Sokaras, D., Harris, H. H., Pickering, I. J., and George, G. N. (2020) Solution chemistry of copper(II) binding to 8-hydroxyquinolines, *Inorg. Chem.* *59*, 13858–13874. DOI: 10.1021/acs.inorgchem.0c01356
12. Kenche, V. B., Zawisza, I., Masters, C. L., Bal, W., Barnham, K. J., and Drew, S. C. (2013) Mixed ligand Cu<sup>2+</sup> complexes of a model therapeutic with Alzheimer's amyloid- $\beta$  peptide and monoamine neurotransmitters, *Inorg. Chem.* *52*, 4303-4318.
13. Mital, M., Zawisza, I., Wiloch, M. Z., Wawrzyniak, U. E., Kenche, V. B., Wróblewski, W., Bal, W., and Drew, S. C. (2016) Copper exchange and redox activity of a prototypical 8-hydroxyquinoline: Implications for therapeutic chelation, *Inorg. Chem.* *55*, 7317-7319.
14. Ballardini, R., Varani, G., Indelli, M. T., and Scandola, F. (1986) Phosphorescent 8-quinolinol metal-chelates - Excited-state properties and redox behavior, *Inorg. Chem.* *25*, 3858-3865.
15. Goldman, M., and Wehry, E. L. (1970) Environmental effects upon fluorescence of 5- and 8-hydroxyquinoline, *Anal. Chem.* *42*, 1178-1185.
16. Yang, L., Powell, D. R., and Houser, R. P. (2007) Structural variation in copper(I) complexes with pyridylmethylamide ligands: Structural analysis with a new four-coordinate geometry index,  $\tau_4$ , *Dalton T.*, 955-964.
17. Okuniewski, A., Rosiak, D., Chojnacki, J., and Becker, B. (2015) Coordination polymers and molecular structures among complexes of mercury(II) halides with selected 1-benzoylthioureas, *Polyhedron* *90*, 47-57.